JME

Geochemistry, petrology, and mineralization in volcanic rocks located in south Neyshabour, NE Iran

A. Entezari Harsini[1], S.A. Mazaheri[1*], S. Saadat[2], J.F. Santos[3]

1. *Department of Geology, Ferdowsi University of Mashhad, Mashhad, Iran*
2. *Department of Geology, Mashhad Branch, Islamic Azad University, Mashhad, Iran*
3. *Department of Geosciences, Geobiotec Research Unit, University of Aveiro, Aveiro, Portugal*

Abstract

This paper presents the new geochemical isotopes Sr and Nd, and the mineralization data for the south Neyshabour volcanic rocks located in NE Iran. Based on the chemical classifications, the studied rocks are basaltic trachy andesite, trachy andesite, trachyte, and trachy dacite in composition. All the analyzed volcanic rocks display enrichment in light rare earth elements (LREE) relative to the heavy rare earth elements (HREE), have significant negative Ti and Nb anomalies, and have a positive U anomaly. The tectonic discrimination diagrams for the volcanic rocks in the studied area show a post-collisional arc environment. These characteristics are the specifications of the subduction-related volcanic rocks generated in a post-collisional setting. The initial $^{87}Sr/^{86}Sr$ ratios ranging from 0.70408 to 0.70593 and the εNdi values between +3.34 and +5 for the four samples analyzed indicate that the studied rocks are derived from a lithospheric mantle source. Finally, it is concluded that these volcanic rocks should have formed in a post-collisional environment that followed the Neo-Tethys subduction. There are strong evidence for copper mineralization in these volcanic rocks. The main copper oxide minerals are malachite and atacamite. The copper sulfide minerals such as chalcocite, minor bornite, and covellit are also present. Chalcocite is the most abundant sulfide ore mineral present in this area. This mineralization is observed as open space filling and thin veinlets, and it is partially controlled by linear structures and fault zones. Based on the identified characteristics, this ore deposit is hydrothermal. Carbonate alteration is frequently seen in the area but argillic alteration is very low, and this issue displays a hydrothermal solution with an alkaline pH.

Keywords: *Chalcocite, Post-Collision Volcanic Rocks, Sr And Nd Isotopes, Neyshbour, NE Iran.*

1. Introduction

The volcanic rocks in Iran are mainly classified into three geographical categories, as follows: a belt extended from the Maku area to the Bazman zone, the Alborz Mountains, and the east territories of Iran [1]. These rocks are mainly andesitic in composition but the other types of volcanic rocks such as rhyolite, dacite, trachyte, and basalt\ are also present [1]. Continental collision results in an extensive magmatic activity not necessarily related to the widespread extension or orogenic collapse. This activity has been termed as the 'post-orogenic' [2] or 'collision zone' [3] magmatism. The production

of collision zone magmas is commonly linked with lithospheric thinning [2, 4] or the mantle upwelling following break-off of the down-going oceanic slab [5]. Magmatism has also been associated with dewatering of hydrous phases in the lithospheric mantle [3, 6], melting of deeply-subducted continental crust, and small-scale sub-lithospheric convection [7]. The Turkish-Iranian Plateau was formed in the Late Cenozoic across what is now Eastern Anatolia (Turkey), Southern Georgia, Armenia, Azerbaijan, and Iran as a response to the Arabia-Eurasia collision. The region is a prime site for the study

of collision magmatism, being a young part of the Alpine–Himalayan belt with abundant and reasonably well-studied volcanic and intrusive rocks. There is also an ever-improving geophysical dataset that can be used to link magmatism to the geodynamic processes [8-10]. Most collision magmatism in the plateau has an incompatible element-enriched calc-alkaline or shoshonitic signature with trace element evidence for the presence of subduction-modified lithosphericmantle sources [4, 11-12]. Magmatic activity has been variously linked to the processes above [3, 4, 6, 7, and 12]. The studied area is located 220 km SW of Mashhad (capital of the Khorasan Razavi province in NE of Iran) and 80 km south of Neyshabour (a city in the Razavi Khorasan province). The area extends from 58° 42' 15" to 58° 43' 40" east longitude and 35° 47' 30" to 35° 52' 00" north latitudes, equivalent to 48 km² (Figure 1). This region is located in the NE of the central Iran zone and inside the Sabzevar structural zone north of the Daruneh fault [13, 14-15]. There are some chromite ore deposits in the ophiolitic rocks in the Sabzevar structural zone. In addition, volcanic and intrusive rocks that have large outcrops in this area indicate mineralization of copper, copper-gold (such as Abbasabad region), gold (such as Koohzar Damghan and Gandi regions), and copper-lead-zinc mineralization. This paper presents new data for the mineralization and petrochemical characteristics of the Sr and Nd isotopes, which can provide a mineralization and petrogenetic model from magmatism in this area.

2. Method
2.1. Preparation of samples
More than 183 thin sections, 10 thin polished sections, and 10 polished blocks were prepared in the laboratory of the Ferdowsi University of Mashhad for the petrography, mineralization, and alteration studies. The samples were collected from the surface. The location of samples presented in Figure 2.

2.2. Major and trace element geochemistry
According to the petrographic studies, twenty samples of unaltered rocks were selected for chemical analysis. The selected samples were crushed and powdered using mild steel, and sent to Kansaran Binaloud Company (Tehran, Iran) for measuring the major elements by XRF. Moreover, the samples were sent to Acme laboratories (Vancouver, Canada) for trace element analysis by ICP mass spectrometry, which was carried out based on the lithium metaborate-tetraborate fusion and nitric acid digestion.
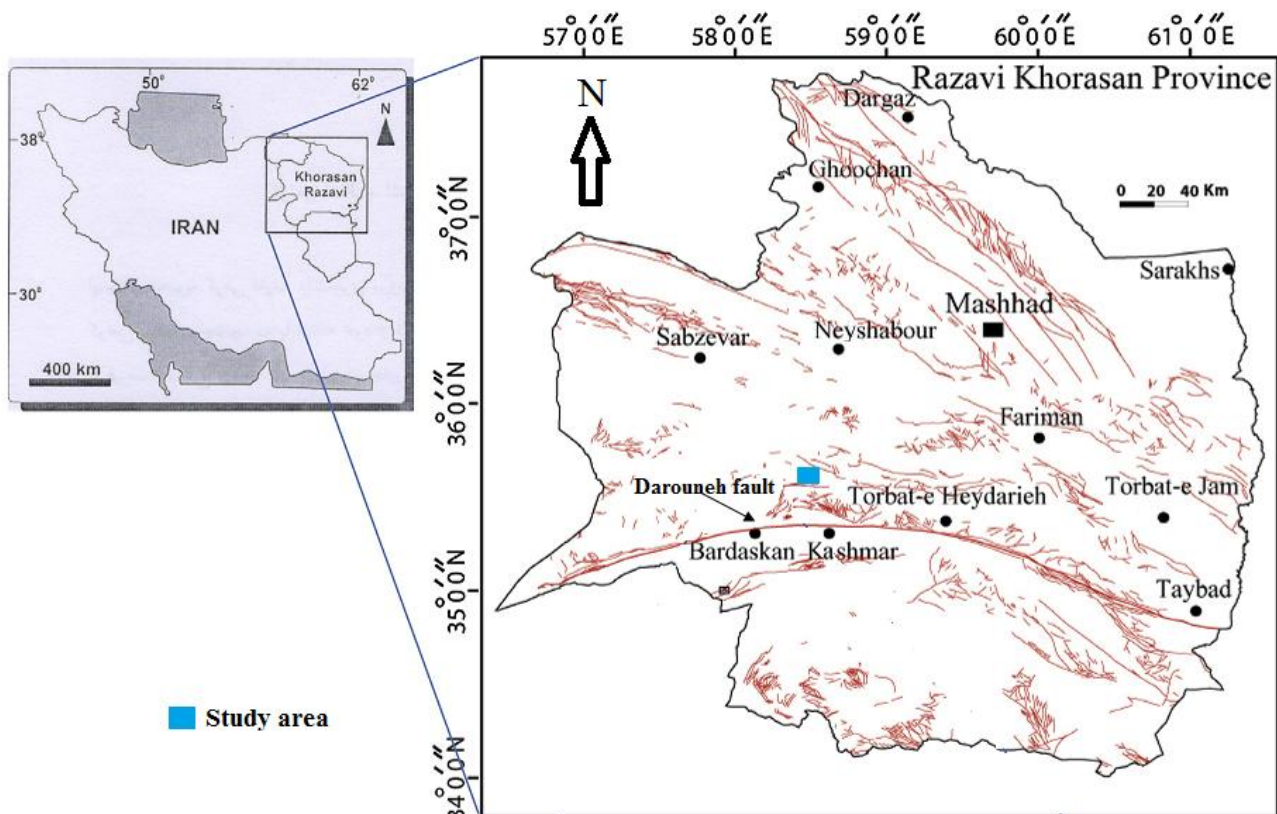

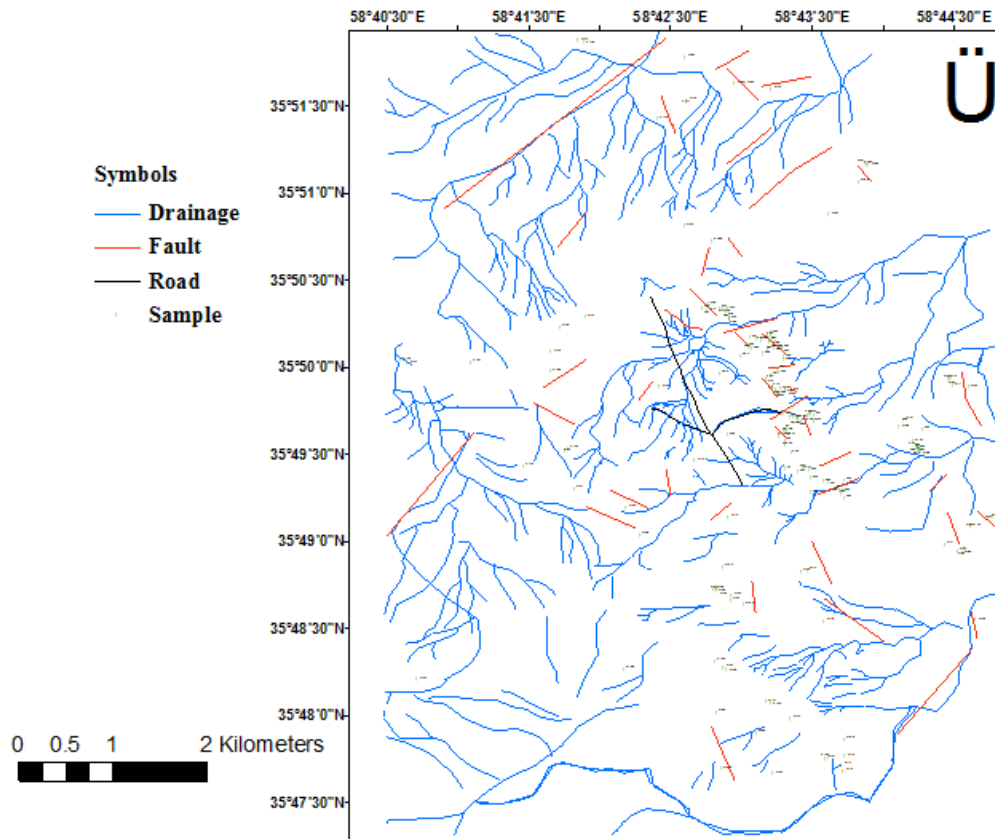**Figure 1. Location of studied area in NE Iran.**

Figure 2. Location of samples in rock units from south Neyshabour area.

2.3. Sr and Nd isotopic analysis

Based on the petrographic studies and geochemical information, four samples from the volcanic rocks with low LOI and minimum alteration were selected and sent to the Laboratory of Isotope Geology of the Aveiro University (Portugal) for determination of the Sr and Nd isotope compositions.

3. Results

3.1. Petrography

Based on the petrographical observations, the studied volcanic rocks indicate porphyritic textures with phenocrysts of plagioclase,

K-feldespar, opacity hornblende, pyroxene, and magnetite, embedded in a fine-to-medium-grained groundmass. Moreover, the amygdaloidal and poikilitic textures were seen in thin sections (Figure 3). Based on the assemblage of the minerals and their percentage, the volcanic rocks of this area can be divided into 9 groups, including: Hornblende pyroxene olivine andesite basalt, Olivine hornblende andesite basalt, Pyroxene hornblende trachy andesite, Hornblende pyroxene trachy andesite, Hornblende andesite, Andesite, Hornblende trachy andesite, Trachy andesite and Pyroxene andesite (Figure 4.)

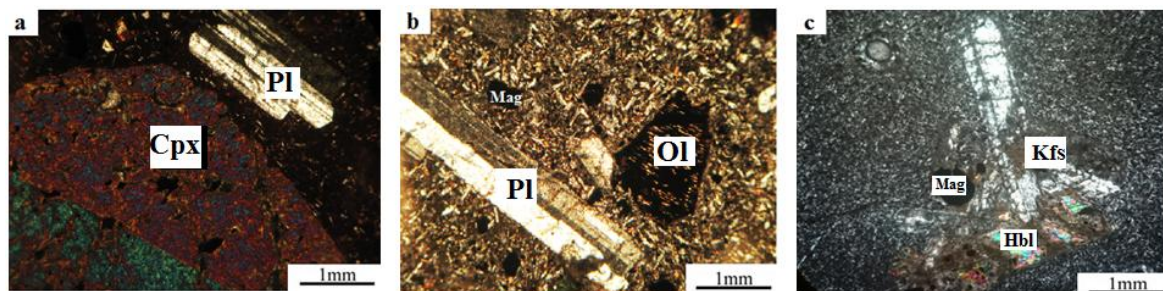**Figure 3. Photomicrographs of thin sections from volcanic rocks in studied area, XPL: (a) Plagioclase and pyroxene phenocrysts in microlitic groundmass (b) Plagioclase and olivine phenocrysts in fine-grained groundmass (c) K-feldspar, hornblende, magnetite phenocrysts, and glomeroporphyritic texture (Pl=Plagioclase; Cpx=Clinopyroxene; Ol=Olivine; Kfs=K-feldspar; Hbl=Hornblende; Mag=Magnetite).**
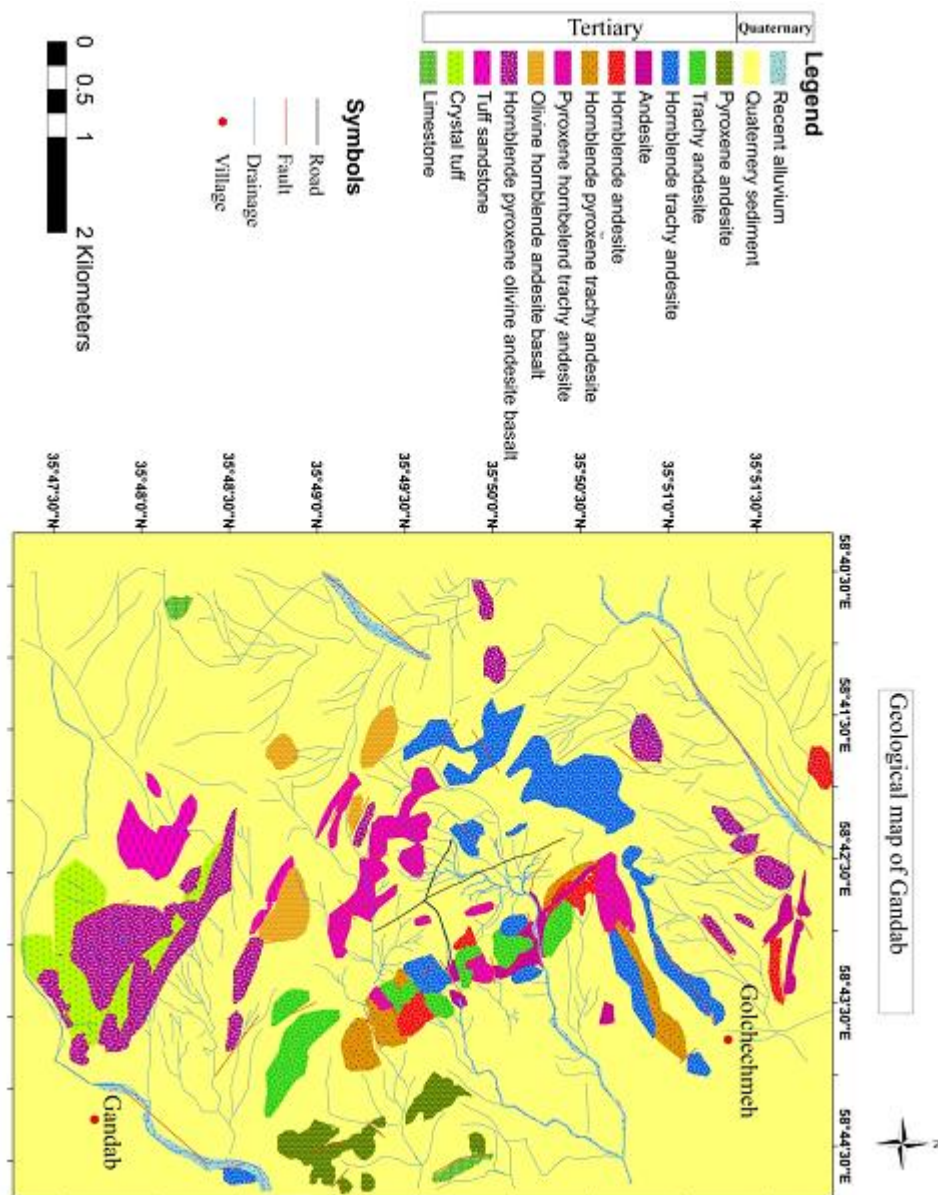
Figure 4. Geological map of studied area.

3.2. Major, trace, and rare earth elements; geochemistry

Table 1 indicates the symbols and locations of the samples. The results obtained for the major and trace elements for 20 samples of no to slightly-altered volcanic rocks are presented in Table 2. The total alkali-silica (TAS) classification diagram [16] is used to categorize the volcanic rocks. These samples were plotted within the basaltic trachy andesite, trachy andesite, trachyte, and trachy dacite fields (Figure 5a). Most of the samples were located in the alkaline section and boundary of alkaline and sub-alkaline field [17] (Figure 5b), and their geochemical character with alumina saturation index [ASI = molar $Al_2O_3/(CaO + K_2O + Na_2O)$]

is ranged from 0.71 to 1.02. Using SiO_2 as a fractionation index, the MgO, FeO, and CaO contents displayed negative correlation with SiO_2 content, while the Al_2O_3, K_2O, and Na_2O contents represented positive correlation with SiO_2 content; moreover, TiO_2 and P_2O_5 were dispersed, and they showed no correlation with the SiO_2 content (Figure 6 a-h). The linear trends among SiO_2 and several major oxides demonstrates a genetic relationship in these volcanic rocks. Along with increasing the silica content, CaO, MgO, and FeO decreased in these rocks. Probably such trends are compatible with fractionation of the phenocryst phases observed, which were derived from a basaltic andesite as a parental magma. In fact, this type of variation displays that Mg- and Fe-rich

rock-forming minerals contain amphibole, pyroxene, and olivine, so they have played a great role during crystallization of the volcanic rocks (mafic minerals like olivine and pyroxene are crystallized early in the process that results in removing Mg, Fe, and Ca, and enrichment of liquid in silica) like plagioclases, and represents the effect of fractional crystallization on a pending magmatic evolution. As plagioclase forms a continuous solid solution between albite ($NaAlSi_3O_8$) and anorthite ($CaAl_2Si_2O_8$), the crystallization temperature changed. Anorthite has a higher crystallization temperature, so the early formed plagioclase crystals are Ca-rich. As Ca is used up in the melt, the crystallizing plagioclase becomes progressively more Na-rich. Na_2O, Al_2O_3, and *K_2O vs. SiO_2* diagrams display a positive trend. This issue points out that K-feldspar and sodic plagioclases (Na rich plagioclase) were crystallized in the late stage of the crystallization and fractionation of a silicate melt in low pressures. The increasing amount of Al_2O_3 is due to their more participation in feldspars. During the fractional crystallization of the magma, the incompatible elements such as the La, Nb, Zr, Rb, Th, Ta, and Hf contents increased with increasing SiO_2 concentrations (Figure 6 i-o). The incompatible trace element variations in these igneous rocks are in agreement with plagioclase and amphibole [18]. As a result, the crystal fractionation process is specified from the parental magma. The trace element of the samples was normalized to primitive mantle [19] (Figure 7a), and indicate that the volcanic rocks are depleted in high field strength elements (HFSE), which may be owing to fractionation of a titanium-rich phase in the magma source [20]. Additionally, all samples have enrichment in the large ion lithophile (LILE). The above-mentioned characteristics point out that the volcanic rocks would belong to the subduction zones. Figure 6b shows a range of chondrite-normalized distribution REE patterns [21] for 20 analyzed samples. The La_N/Sm_N ratios vary between 2.35 and 4.09 (on average, 3.37), which display moderate enrichment in light rare earth elements (LREE). Eu anomaly is calculated by the $Eu/Eu^*=Eu_N/(Sm_N \times Gd_N)^{1/2}$ formula (Taylor and McLennan, 1985). The Eu anomaly values range from 0.72 to 0.97 (on average, 0.87), which represent weakly negative Eu anomaly [22] for the studied samples, and the Gd_N/Yb_N values range from 1.41 to 1.86 (on average, 1.65). These ratios reflect nearly flat heavy rare earth element (HREE) on the normalized REE patterns compared to the chondrite values [23].

Table1. Symbol and location of samples (UTM) of south Neyshabour volcanic rocks.

Symbol	Zone	Lat	Long	Sample
S-119	656119	3962448	40S	⬖
S-154	653057	3968425	40S	⬖
S-131	653768	3965241	40S	⬓
S-179	652671	3965670	40S	⬓
S-144	655354	398326	40S	✳
S- 60	654773	3966669	40S	■
S-17	655352	3966494	40S	■
S-113	655634	3964537	40S	■
S-140	654365	3968353	40S	◆
S-35	654994	3966895	40S	◆
S-160	652970	3966897	40S	◆
S-183	655638	3965998	40S	◆
S-158	652970	3966879	40S	◆
S-157	654126	3966522	40S	◆
S-16	655416	3966508	40S	▲
S-71	655737	3966255	40S	▲
S- 40	655269	3966919	40S	▲
S- 31	655092	3967049	40S	▲
S-57	654632	3967377	40S	+
S- 86	655994	3965417	40S	+
S-171	657228	3964983	40S	⊕
S-92	657265	3964785	40S	⊕

Table 2. Major, trace, and rare earth element analysis of south Neyshabour volcanic rocks.

Sample	S-171	S-92	S-119	S-153	S-131	S-179	S-60	S-17	S-140	S-35	S-160	S-183	S-16	S-71	S-57	S-86	S-40	S-31	S-27	S-49
SiO$_2$	62.58	61.54	54.01	54.39	55.01	54.56	57.86	57.12	57.71	57.35	58.01	57.25	57.86	57.42	60.88	59.35	58.36	58.12	55.87	55.12
Al$_2$O$_3$	17.69	17.59	15.91	16.05	15.86	15.62	17.99	18.03	18.24	18.35	18.02	18.42	17.08	16.89	17.52	18.13	17.63	17.51	15.24	15.35
FeO	3.50	3.82	8.21	7.92	7.53	7.79	4.80	5.35	5.19	5.12	5.23	5.17	5.21	5.34	3.73	4.22	4.85	5.01	4.26	4.78
CaO	5.27	5.92	6.87	6.52	7.02	7.32	4.26	4.62	5.17	5.21	5.24	5.27	2.86	3.42	1.68	1.89	3.01	2.97	4.98	5.02
Na2O	4.48	4.53	3.56	3.45	3.29	3.35	4.34	4.12	3.94	4.25	3.59	3.75	4.75	4.35	4.26	4.12	3.87	3.67	2.98	2.87
K$_2$O	3.02	2.95	2.99	3.25	3.38	3.57	5.49	5.15	4.02	3.98	4.08	3.92	6.89	6.72	7.34	6.95	7.02	6.99	7.41	7.25
MgO	0.27	0.42	5.24	5.10	4.52	4.98	1.78	1.98	2.35	2.37	2.34	2.52	1.69	1.91	1.48	1.79	1.49	1.78	0.98	1.35
Cu	0.02	0.02	0.01	0.01	0.01	0.01	0.02	0.02	0.01	0.01	0.01	0.01	0.05	0.07	0.05	0.06	0.10	0.06	1.69	1.81
TiO$_2$	1.429	1.354	0.891	0.854	0.840	0.915	0.968	1.071	0.869	0.864	0.867	0.862	1.011	1.009	0.914	1.050	0.918	0.899	1.154	1.034
MnO	0.080	0.069	0.112	0.131	0.098	0.082	0.069	0.059	0.045	0.048	0.042	0.046	0.124	0.105	0.040	0.051	0.078	0.087	0.063	0.087
P$_2$O$_5$	0.336	0.392	0.341	0.313	0.362	0.333	0.454	0.521	0.418	0.455	0.418	0.428	0.732	0.792	0.323	0.355	0.513	0.532	0.468	0.423
S	0.009	0.008	0.054	0.057	0.009	0.008	0.012	0.013	0.012	0.015	0.008	0.009	0.018	0.035	0.011	0.019	0.008	0.009	0.017	0.017
L.O.I	1.04	1.15	1.62	1.78	1.87	1.55	1.73	1.76	1.66	1.67	1.85	1.87	1.43	1.66	1.51	1.72	2.03	2.10	4.40	4.65
Total	99.72	99.86	99.82	99.83	99.80	99.71	99.77	99.81	99.64	99.52	99.71	99.53	99.71	99.72	99.74	99.71	99.87	99.76	99.51	99.76
Ba	287	294	383	367	376	381	515	552	482	475	451	453	551	525	485	435	570	552	497	505
Be	2	2	1	2	1	1	2	2	1	2	2	2	1	1	2	1	2	2	4	3
Co	4.3	5.6	27.4	28.2	28.7	29.1	9.8	10.1	12.1	12.8	12.7	13.1	8.0	9.1	4.8	5.2	7.4	6.9	6.1	5.8
Cs	1.1	1.5	1.9	2.4	2.2	2.6	2.9	3.1	1.9	1.5	1.3	1.2	3.3	2.8	3.6	3.2	3.3	2.9	3.0	2.8
Ga	19.6	18.3	16.1	15.9	15.6	16.2	15.1	15.6	18.2	18.8	17.2	16.8	15.5	16.1	16.0	15.5	15.0	14.3	13.7	14.1
Hf	7.5	7.4	2.9	2.8	2.9	2.9	3.7	3.6	3.3	3.5	3.5	3.4	3.6	3.7	4.1	4.2	3.7	3.8	3.4	3.3
Nb	27.9	26.2	9.9	10.4	11.5	10.8	15.2	15.8	14.5	14.1	14.3	14.6	16.5	16.2	19.2	18.8	15.8	15.6	15.3	15.7
Rb	68.0	73.1	70.8	72.4	74.4	79.1	135.4	142.1	97.0	110.2	96.1	82.2	160.4	155.2	182.2	173.1	158.7	148.9	144.9	145.5
Sn	3	2	2	1	1	2	1	1	1	2	1	1	1	1	1	2	2	1	1	1
Sr	453.9	438.2	614.8	580.3	559.8	592.2	608.6	595.1	726.7	717.3	728.7	731.2	504.7	491.2	239.1	251.2	454.3	432.1	347.2	371.1
Ta	1.8	1.6	0.6	0.7	0.7	0.8	0.9	0.8	0.8	0.9	1.0	0.8	1.1	1.0	1.2	1.1	0.9	1.0	1.0	0.9
Th	9.1	9.5	3.7	4.3	4.1	4.8	6.1	6.2	4.9	5.1	5.0	4.8	7.2	6.9	7.8	7.4	6.7	7.1	6.2	6.3
Nb	2.7	2.5	1.1	1.3	1.1	1.2	1.6	1.4	1.4	1.6	1.5	1.4	2.3	2.5	1.1	1.1	2.3	2.4	2.4	2.1
V	112	120	259	262	252	243	298	310	265	256	269	285	395	375	223	259	361	345	279	242
W	1.4	1.6	1.5	1.9	2.9	3.1	1.3	1.7	1.5	1.8	1.7	1.5	1.4	1.6	2.0	1.8	1.8	1.6	3.3	2.7
Zr	306.1	297.3	108.6	121.5	119.8	109.1	157.9	149.1	142.0	138.5	140.9	135.2	167.5	159.5	193.5	185.1	160.0	163.6	148.0	152.1
Y	30.8	31.2	19.3	18.9	19.4	18.8	16.9	17.1	17.1	16.8	17.9	17.2	18.6	18.3	18.0	18.5	17.4	17.1	16.7	17.2

Table 2. Continued

Sample	S-171	S-92	S-119	S-153	S-131	S-179	S-60	S-17	S-140	S-35	S-160	S-183	S-16	S-71	S-57	S-86	S-40	S-31	S-27	S-49
La	36.3	35.2	15.4	15.8	17.1	16.8	22.6	21.7	21.3	21.5	20.9	21.2	24.7	24.1	24.1	23.2	24.1	23.8	23.3	23.9
Ce	76.9	75.2	32.0	33.2	36.0	35.2	42.6	43.2	43.6	41.9	41.6	42.3	48.3	47.9	45.6	44.9	45.7	45.2	45.8	44.9
Pr	8.96	8.52	4.35	4.71	4.62	4.44	5.25	5.37	5.24	5.01	5.14	4.93	5.71	5.54	5.36	5.59	5.72	5.45	5.51	4.89
Nd	35.8	36.4	17.7	18.1	18.6	18.4	19.9	20.2	19.2	18.8	20.2	20.4	22.3	22.6	20.6	19.9	21.4	22.3	22.3	22.5
Sm	7.14	7.01	4.12	3.93	3.88	4.07	3.75	3.83	4.11	3.95	3.99	4.05	4.39	4.09	3.71	3.91	3.86	4.01	4.00	3.89
Eu	1.69	1.58	1.22	1.17	1.15	1.11	1.05	0.98	1.15	1.19	1.15	1.13	1.11	1.15	0.91	1.08	1.18	1.21	1.09	1.12
Gd	6.69	6.35	4.12	3.93	4.22	4.17	3.53	3.61	3.73	3.68	3.80	3.75	3.67	3.86	3.33	3.52	3.49	3.62	3.57	3.49
Tb	1.04	1.11	0.61	0.56	0.65	0.61	0.57	0.59	0.58	0.58	0.59	0.60	0.60	0.63	0.51	0.56	0.58	0.57	0.54	0.55
Dy	5.64	5.23	3.44	3.61	3.74	3.54	2.91	3.11	3.36	3.21	3.23	3.39	3.51	3.33	2.97	3.08	3.32	3.45	3.01	2.96
Ho	1.10	1.05	0.74	0.72	0.75	0.73	0.60	0.62	0.73	0.68	0.69	0.72	0.65	0.63	0.65	0.69	0.63	0.66	0.61	0.67
Er	3.20	3.11	1.81	1.87	1.99	1.92	1.78	1.81	1.90	1.94	1.92	1.95	1.88	1.83	1.90	1.94	2.06	1.98	1.79	1.85
Tm	0.44	0.41	0.30	0.29	0.30	0.30	0.27	0.28	0.27	0.28	0.29	0.29	0.29	0.29	0.29	0.28	0.28	0.27	0.30	0.30
Yb	2.91	2.76	1.95	1.91	1.92	1.89	1.70	1.72	1.84	1.86	1.73	1.87	1.87	1.92	1.91	1.88	1.84	1.87	1.71	1.73
Lu	0.46	0.48	0.31	0.30	0.31	0.31	0.27	0.28	0.29	0.27	0.28	0.29	0.32	0.30	0.31	0.30	0.31	0.31	0.28	0.29
Nb/Th	3.07	2.757	2.68	2.42	2.80	2.25	2.49	2.54	2.96	2.76	2.86	3.04	2.29	2.35	2.46	2.54	2.36	2.2	2.47	2.49
Ba/Sr	0.63	0.67	0.62	0.63	0.67	0.64	0.85	0.93	0.66	0.66	0.62	0.62	1.09	1.06	2.02	1.73	1.25	1.27	1.43	1.36
Th/Yb	3.13	3.44	1.90	2.25	2.14	2.54	3.59	3.6	2.66	2.74	2.89	2.57	3.85	3.59	4.08	3.94	3.64	3.8	3.63	3.64
La/Nb	1.30	1.34	1.56	1.52	1.49	1.56	1.49	1.37	1.47	1.52	1.46	1.45	1.50	1.49	1.25	1.23	1.53	1.53	1.52	1.52
(La/Sm)$_N$	3.20	3.16	2.35	2.53	2.77	2.60	3.79	3.56	3.26	3.42	3.29	3.29	3.54	3.71	4.09	3.73	3.93	3.73	3.66	3.86
Eu/Eu*	0.75	0.72	0.91	0.91	0.87	0.82	0.88	0.81	0.90	0.95	0.90	0.89	0.85	0.88	0.79	0.89	0.98	0.97	0.88	0.93
(Gd/Yb)$_N$	1.85	1.86	1.70	1.66	1.77	1.78	1.68	1.69	1.64	1.60	1.77	1.62	1.58	1.62	1.41	1.51	1.53	1.56	1.64	1.63

3.3. Sr and Nd isotopes

The Sr and Nd isotopic data obtained in the four selected samples are presented in Table 3. These samples have the $^{143}Nd/^{144}Nd$ and $^{87}Sr/^{86}Sr$ ratios ranging from 0.512807 to 0.512893 and from 0.704082 to 0.705931, respectively. If the Nd isotopic ratio composition is expressed using the εNd notation, the range goes from +3.3 to +5.0. For Sr and Nd, the isotopic ratios and εNd values show insignificant differences between the present-day values and the calculated initial values for young geological ages like those obtained in this work (less than 6 Ma) since both ^{87}Rb and ^{147}Sm have very low decay constants [24, 25]. Therefore, the measured isotopic ratios, in this case, may be considered, in practical terms, as representing the initial compositions.
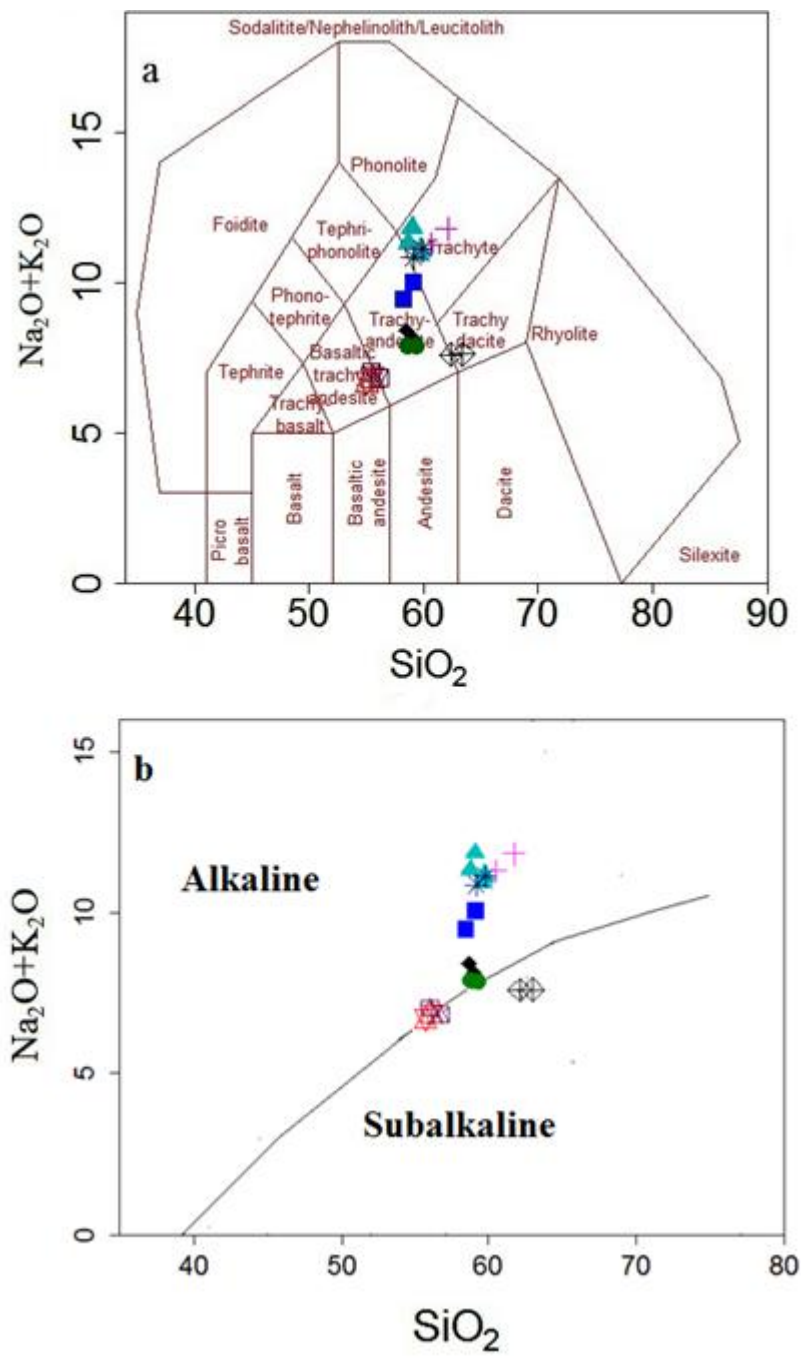
Figure 5. (a) Na₂O + K₂O vs. SiO₂ diagram for classification of volcanic rocks [16]; (b) Na₂O + K₂O vs. SiO₂ diagram to distinguish between subalkaline and alkaline fields [17].
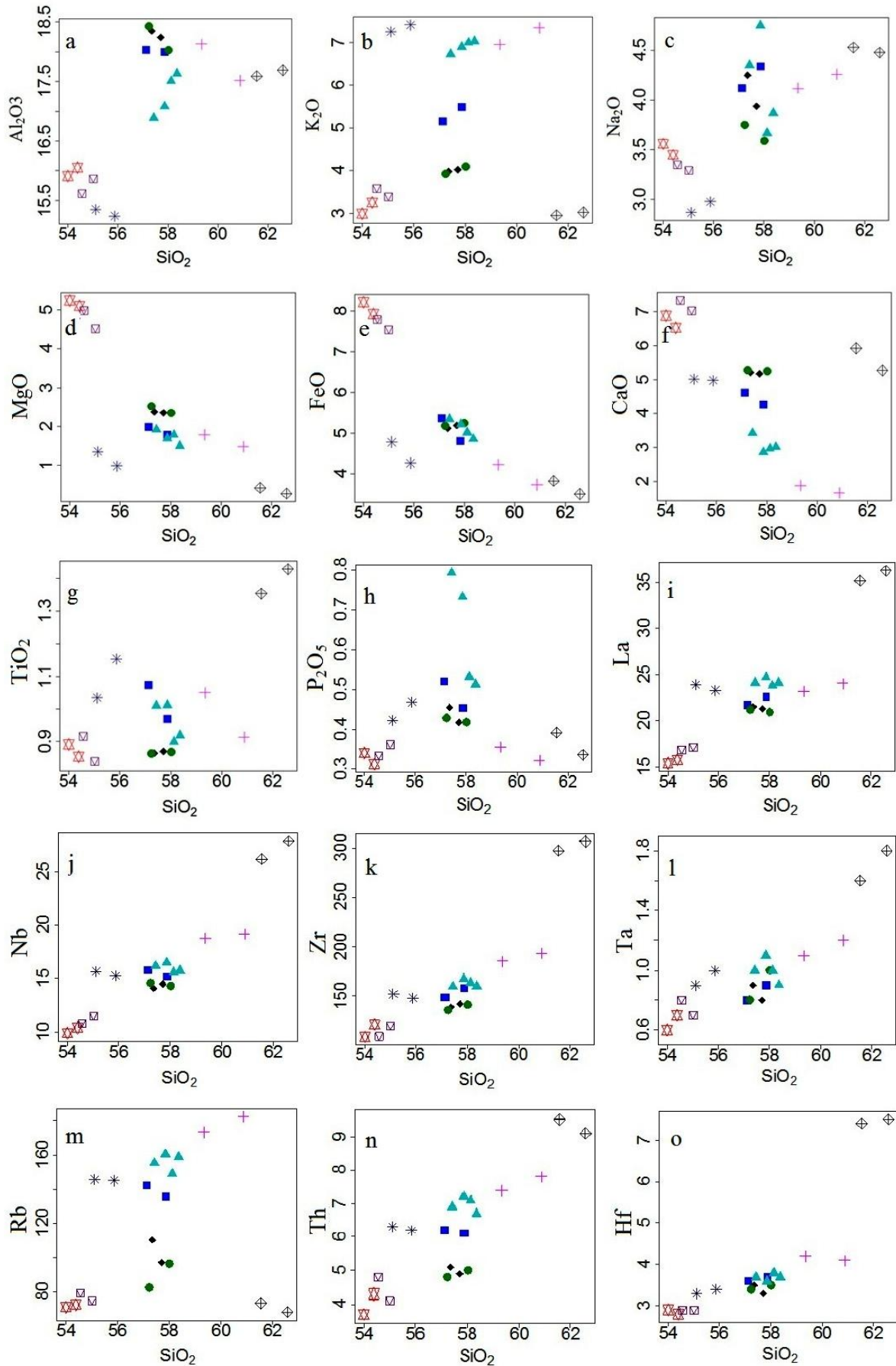
Figure 6. Selected major and trace elements *vs. SiO₂* contents for the south Neyshabour volcanic rocks.
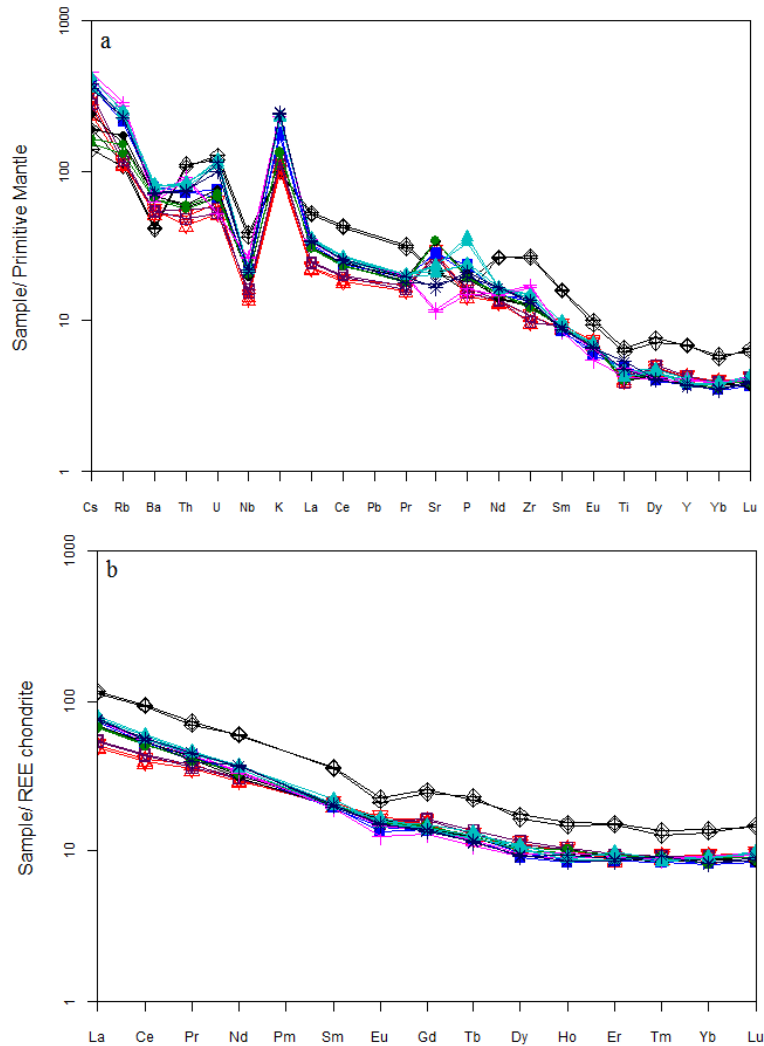
Figure 7. (a) Primitive-mantle normalized diagrams [30]; (b) REE chondrite normalized [32].

Table 3. Rb–Sr and Sm–Nd isotopic data for south Neyshabour volcanic rocks.

Sample	Rb (ppm)	Sr (ppm)	$^{87}Rb/^{86}Sr$	$^{87}Sr/^{86}Sr$	error (2σ)	Sm(ppm)	Nd(ppm)	$^{147}Sm/^{144}Nd$	$^{143}Nd/^{144}Nd$	error (2σ)	εNd
S- 16	106	505	0.609	0.705047	0.000020	4.39	22.3	0.119	0.512833	0.000017	+3.8
S- 57	182	239	2.205	0.705931	0.000020	3.71	20.6	0.109	0.512807	0.000015	+3.3
S-171	68.0	454	0.433	0.704082	0.000021	7.14	35.8	0.121	0.512893	0.000015	+5.0
S-119	70.8	615	0.333	0.704614	0.000016	4.12	17.7	0.141	0.512843	0.000017	+4.0

4. Discussion

4.1. Source properties

The negative and positive εNd(t) isotopic ratios demonstrate the features of the crustal melt and mantle array, respectively [26, 27]. With respect to the εNdi–($^{87}Sr/^{86}Sr$)i isotopic data depicted in Figure 8, the south Neyshabour volcanic rocks show a trend toward the mantel [26]. These samples are mainly characterized with high concentrations of the incompatible trace elements (e.g. LILE and LREE). Moreover, Figure 5 also shows that these samples are marked by considerable negative Nb, Ta, and Ti anomalies, specifying that the samples have not been driven from normal MORB or OIB mantle sources,

which usually demonstrate positive Nb-Ti anomalies in primitive-mantle normalized trace element diagrams [28]. Moreover, the Nb/La ratios of the south Neyshabour volcanic samples were changed from 0.64 to 0.79, representing a lithospheric mantle source [11, 29]. Thus these volcanic rocks have possibly been derived from an enriched mantle source containing a distinct subduction signature. The trace-element compositions of the south Neyshabour volcanic rocks (NE Iran) also indicate that their parental magma was produced by generally low degrees of partial melting. The $(La/Yb)_N$ value for these samples varied from 5.32 to 9.31. This ratio was less than the $(La/Yb)_N$ ratio in the igneous rocks,

which have been derived from the magma with garnet ((La/Yb)N > 20) as the major phase in their source [6, 11, 30], representing the garnet as the major residual phase. Therefore, spinel and/or amphibole may exist in the residua phase. Nevertheless, the slight enrichment in MREE of the samples (Figure 7) indicates that amphibole may not stay stable in the residual following fractional melting [30, 31]. La/Yb versus Yb is also useful to assess the degree of mantle partial melting and distinguish between melting in the spinel and garnet fields [31-33]. There is a very small change in the La/Yb ratio in the spinel-facies melts compared with their mantle source. In contrast, there are large changes in Yb in the melts formed in garnet-facies mantle [31, 33]. Based on the La/Yb ratio and the amount of Yb of south Neyshabour volcanic rocks, neither a variables degree of partial melting in a spinel lherzolite nor a variables degree of partial melting of garnet lherzolite solely can generate the observed variation in the La/Yb ratio by changing Yb. One possible explanation for the La/Yb versus Yb compositions of these volcanic rocks involves mixing of small melt fraction from garnet-facies mantle with a relatively larger melt fractions from the spinel-facies mantle.
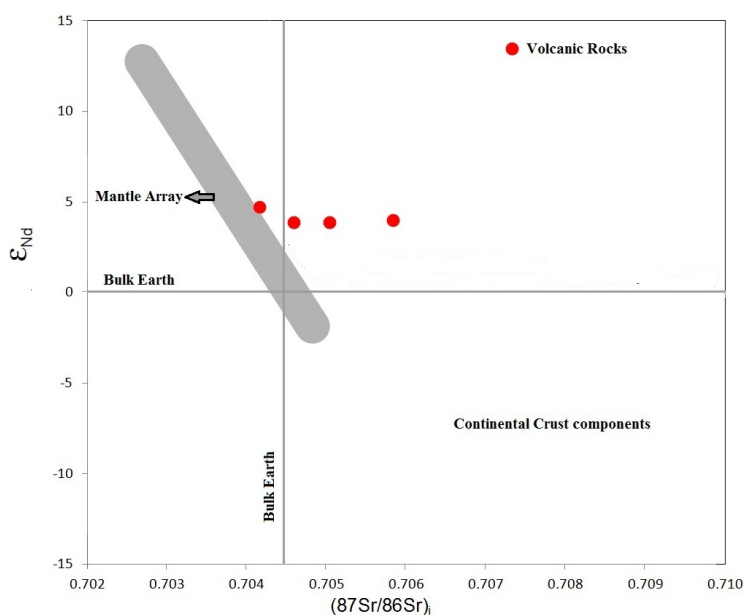
Figure 8. Plot of initial ($^{87}Sr/^{86}Sr$) i vs. $^{\varepsilon}Nd$ ratios.

4.2. Tectonic setting

Application of TiO_2 *vs.* Al_2O_3 [34] indicates that all samples are placed in the arc environment (Figure 9a). Plotting the samples on the Nb * 50-Zr*/3-Ce/P_2O_5 ternary diagram [34] shows that the south Neyshabour volcanic rocks are situated at post-collisional arc (Figure 9b). Researchers [e.g. 35] have used the Nb/Th ratio to survey the effect of subduction zone processes on the formation of the volcanic rocks. This ratio is lower than '4' in the rocks related to the subduction zone [19]. The Nb/Th ratio of the proposed samples changed from 2.19 to 3.06. As a result, the Nb/Th ratio in the proposed samples is less than '4', and this verifies that the studied rocks were affected by the processes related to the subduction zone. As mentioned earlier, the studied area is located in the Sabzevar zone (NE Iran). During the Late Cretaceous, the Sabzevar oceanic basin (branch of the Neo-Tethys Ocean between central Iranian micro-continent and Eurasian margin) was formed, and then it closed during Paleocene-Eocene [36]. With regard to the geochemical properties and tectonic environment of the south Neyshabour volcanic rocks, we believe that they were created in the post-collision environment after the closure of this branch of Neo-Tethys. Enrichment in LILE and LREE relative to HFSE and HREE, respectively, and negative anomalies of the Nb and Ti elements are the specifications of the subduction-related magmas. These characteristics are generally related to a mantle source, which has already been enriched in LILE and LREE over HFSE and HREE by the metasomatic activity of fluids released from the subducted sediments or oceanic slab [37, 38]. Many different types of models have been suggested to illustrate this signature in the

post-collisional setting such as considering amphibolites, peridotite, and metapelite as a hybrid source in the crust–mantle boundary [39] or presenting a theory regarding mixing of magmas in the asthenosphere and enriched lithospheric mantle [40]. Considering all evidence, the best suggestion can be an enrichment of the lithospheric mantle by earlier subduction events in a post-collision stage [41].
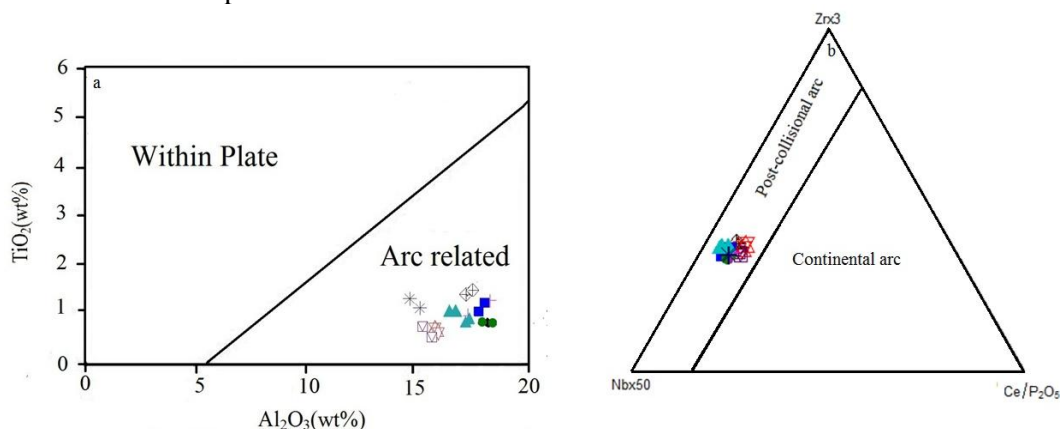

Figure 9. (a) *TiO₂ vs. Al₂O₃* **binary diagram to separate within plate environment and arc related, [34]; (b) Nb*50-Zr*/3-Ce/P2O5 ternary diagram to separate continental arc and post-collisional arc [34].**

4.3. Mineralization

Carbonate and chlorite minerals are of malachite and atacamite, respectively, and sulfide mineral of chalcocite, minor bornite, and covolite are seen on the surface of the studied volcanic rocks. Copper minerals are seen in association with volcanic rocks at all sections of the area; these minerals have mainly filled the thin veinlets and voids. Figure 10 shows this issue. Mineralogical findings were checked by the XRD test (Figure 11). In XRD, the results were discriminated minerals of malachite, atacamite, and chalcocite but covolite and bornite were not detected because of their small amount in the samples. The main sulfide ore mineral in this region is chalcocite. Enormous amounts of chalcocite, not a high amount of Fe oxide and bornite, in the region show that chalcosite is mainly from the first generation, and in the second generation, it is lower than what probably formed from the conversion of bornite. There is also the possibility that large quantities of chalcocites changed into malachite and atacamite under the oxidizing conditions by meteoric waters. However, copper minerals were formed in two phases. The first mineralization phase was calchocite with minor bornite, and the secondary phases had more malachite and atacamite and low chalcocite and covellite (Figure 12). The suitable space for transferring mineralizer solutions is provided by pores in rocks and rock joints, which have cut the host rocks in different directions. In addition, the mineralization is seen as leakage and replacement in some places. In some parts of the region, there are certain evidence that copper-bearing solutions are controlled by linear structures and fault zones. According to the composition and texture of the wall rocks and solution volume, this feature occurred from a few centimeters to several meters in the host rock. In the near of the faults and contacts between two units of rocks, large amounts of mineralization and carbonate alteration was observed, and this alteration shows an alkaline pH. The primary chalcosite is formed in low sulfur and Eh conditions. Pyrite mineralization is absent in the studied area, and this issue represents that the amount of iron is low in the mineralizer solutions. Along with get away from the faults and moving toward the upper rock units, the mineralization evidence disappeared or limited. Based on the identified characteristics, this deposit is a hydrothermal ore deposit whose solutions have alkaline pH and low iron, sulfide, and Eh. Copper sulfide mineralization depends on the parent magma, which has analkaline nature with good differentiation. In the fluid phase, because of the alkaline nature, its residue has many Na and Ca ions with ore-forming cations, so their derived solutions have high pH. Based on the petrographic studies, the south Neyshabour volcanic rocks have a high magnetite but they do not show the origin of mineralization if they are the origin of mineralization. For a high Fe in magma, we should see pyrite in the mineralization zone but the absence of pyrite shows that we need drilling at depth for finding its origin.
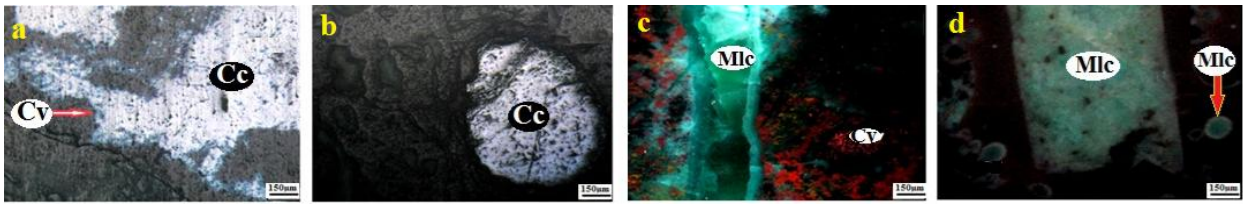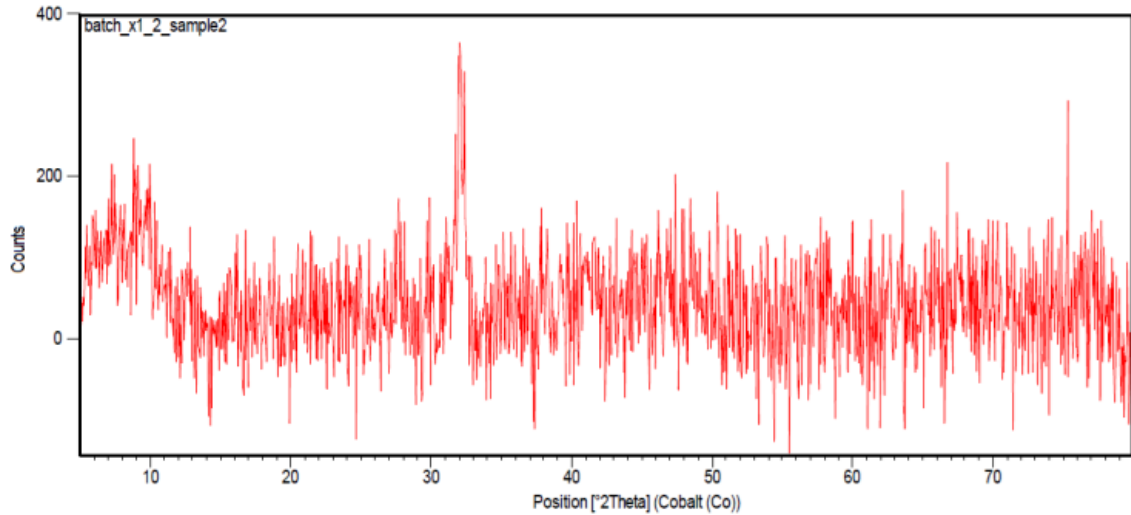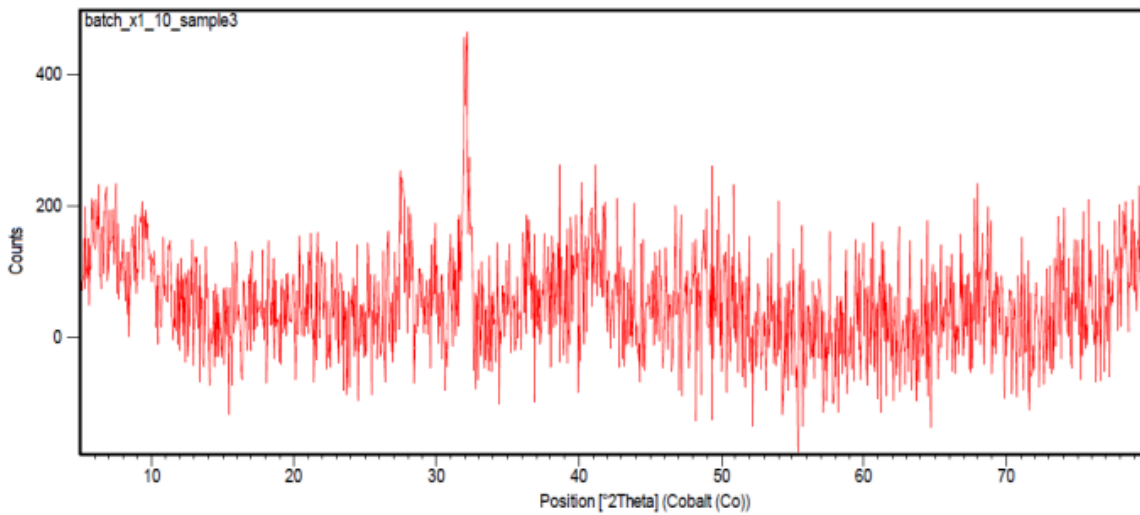
Figure 10. (a) Chalcocite into veinlet is converted to covollite, PPL; (b) Chalcocite into void,PPL; (c) Malachite into veinlet, XPL; (d) Malachite into voids, PPL. (Cc= Chalcocite; Cv= Covollite; Mlc= Malachite).

Figure11. Results of XRD test.

Figure 12. Paragenetic sequence of copper mineralization in studied area.

5. Conclusions

Based on the total alkali-silica (TAS) classification diagram, the volcanic rocks in the studied area are basaltic trachy andesite, trachy andesite, trachyte, and trachy dacite; they have been formed from the same magma by the crystal fractionation process. In primitive mantle and chondrite-normalized trace element spider diagrams, the analyzed samples demonstrate slight-to-moderate enrichment in LILE ($2.35 \leq La_N / Sm_N \leq 4.09$) compared with HFSE ($1.41 \leq Gd_N / Yb_N \leq 1.86$), while being accompanied by the negative anomalies of Nb and Ti. These geochemical properties and the isotope geochemistry (Sr_i and $^{\varepsilon}Nd_i$) illustrate that the studied rocks are derived from a metasomatized lithospheric mantle source. The analyzed samples show a post-collisional arc environment. We suggest that the volcanic activity in the studied area after Eocene period has been created by the enriched lithospheric mantle source, which has previously been metasomatized by subducted sediments after Neo-Tethys subduction. Based on the field and laboratory studies, mineralization in this region occurred in the suitable tectonic setting related andesitic units, and the active tectonic plates caused the formation of joint systems, cracks, veins, veinlets, and fractures in rocks. These have turned into channels for the infiltration of copper-bearing solutions from the depths to the surface resulting in the expansion of copper mineralization in the region. Minerals of malachaite, atacamite, chalcosite, and minor bornite and covollite are observed in this area. Based on our studies, mineralization in this area is of hydrothermal type, and the sulfide minerals have been formed under reduction conditions, low sulfur, and alkaline PH, and finding its origin requires drilling in depth.

References

[1]. Pazirandeh, M. (1973). Distribution of volcanic rocks in Iran and a preliminary discussion of their relationship to tectonics. Bulletin Volcanologique. 37: 573-585.

[2]. Turner, S., Arnaud, N., Liu, J., Rogers, N., Hawkesworth, C., Harris, N., Kelley, S., Van Calsteren, P. and Deng, W. (1996). Post-collision shoshonitic volcanism on the Tibetan Plateau: implications for convective thinning of the lithosphere and the source of ocean island basalts. Journal of Petrology. 37: 45-71.

[3]. Allen, M.B., Kheirkhah, M., Neill, I., Emami, M.H. and McLeod, C.L. (2013). Generation of arc and ithin-plate chemical signatures in collision zone magmatism:quaternary lavas from Kurdistan Province, Iran. J. Petrol. 54: 887-911.

[4]. Pearce, J.A., Bender, J. F., Delong, S.E., Kidd, W.S.F., Low, P.J., Guner, Y., Sargolu, F., Yilmaz, Y., Moorbath, S. and Mitchell, J.G. (1990). Genesis of collision volcanism in eastern Anatolia, Turkey. J. Volcanol. Geoth. Res. 44: 189-229.

[5]. Davies, J.H. and Blanckenburg, F. (1995). Slab breakoff: a model of lithosphere detachment and its test in the magmatism and deformation of collisional orogens. Earth Planet. Sci. Lett. 129: 85–102.

[6]. Kheirkhah, M., Neill, I., Allen, M.B. and Ajdari, K. (2013). Small-volume melts of lithospheric mantle during continental collision: late Cenozoic lavas of Mahabad, NW Iran. J. Asian Earth Sci. 74: 37-49.

[7]. Kaislaniemi, L., Van Hunen, J., Allen, M.B. and Neill, I. (2014). Sublithospheric small-scale convection: a mechanism for collision magmatism. Geology. 42: 291-294.

[8]. Angus, D.A., Wilson, D.C., Sandvol, E. and Ni, J.F. (2006). Lithospheric structure of the Arabian and Eurasian collision zone in eastern Turkey from S-wave receiver functions. Geophys. J. Int. 166: 1335-1346.

[9]. Zor, E. (2008). Tomographic evidence of slab detachment beneath eastern Turkey and the Caucasus. Geophys. J. Int. 175: 1273-1282.

[10]. Priestley, K., McKenzie, D., Barron, J., Tatar, M. and Debayle, E. (2012). The Zagros core: deformation of the continental lithospheric mantle. Geochemistry, Geophysics, Geosystems. 13 (11). DOI: 10.1029/2012GC004435.

[11]. Dilek, Y., Imamverdiyev, N. and Altunkaynak, S. (2010). Geochemistry and tectonics of Cenozoic volcanism in the Lesser Caucasus (Azerbaijan) and the peri-Arabian region: collision-induced mantle dynamics and its magmatic signature. Int.Geol. Rev. 52: 536-578.

[12]. Neill, I., Meliksetian, Kh., Allen, M.B., Navasardyan, G. and Karapetyan, S. (2013). Pliocene-Quaternary volcanic rocks of NW Armenia: magmatism and lithospheric dynamics within an active orogenic plateau. Lithos. 180-181: 200-215.

[13]. Ruttner, A. and Stöcklin, J. (1967). Geological map of Iran, scale 1:100,000. Geological Survey of Iran.

[14]. Berberian, M. and King G.C.P. (1981). Towards a paleogeography and tectonic evolution of Iran. Canadian Journal of Earth Sciences. 18: 210-265.

[15]. Alavi M. (1991). Tectonic map of the Middle East, scale 1:2,900,000. Geological Survey of Iran.

[16]. Middlemost, E.A.K. (1994). Naming materials in the magma/igneous rock system, Earth Science Reviews1. 37: 215-224.

[17]. Irvine, T.N. and Baragar, W.R.A. (1971). A guide to the chemical classification of the common volcanic rocks. Canadian Journal of Earth Science. 8: 523-548.

[18]. Mazhari, S.A., Amini, S., Ghalamghash, J. and Bea, F. (2011). Petrogenesis of granitic unit of Naqadeh complex, Sanandaj-Sirjan Zone, NW Iran. Arabian Journal of Geosciences. 4 (1-2): 59-67.

[19]. McDonough, W.F. and Sun, S.S. (1995). Composition of the Earth,Chemical Geology. 120: 223-253.

[20]. Ghalamghash, J., Bouchez, J.L., Vosoughi-Abedini, M. and Nédélec, A. (2009). The Urumieh Plutonic Complex (NW Iran): Record of the geodynamic evolution of the Sanandaj- Sirjan zone during Cretaceous times- Part II: Magnetic fabrics and plate tectonic reconstruction. Journal of Asian Earth Science. 36: 303-317.

[21]. Boynton, W.V. (1984). Geochemistry of the rare earth elements: meteorite studies. Chapter in: Developments in Geochemistry. 2: 63-114.

[22]. Ketchum, K.Y., Heaman, L.M., Bennett,G. and Hughesa, D.J. (2013). Age, petrogenesis and tectonic setting of the Thessalon volcanic rocks, Huronian Supergroup, Canada. Precambrian Research. 233: 144-172.

[23]. Li, X.W., Mo, X.X., Yu,X.H., Ding, Y., Huang, X.F., Wei, P. and He, W.Y. (2013). Petrology and geochemistry of the early Mesozoic pyroxene andesites in the Maixiu Area, West Qinling, China: Products of subduction or syn-collision?. Lithos. 172-173: 158-174.

[24]. Steiger, R.H. and Jäger, E. (1977). Subcommision on geochronology: convention in the use of decay-constants in geo- and cosmochemistry. Earth and Planetary Science Letters. 36: 359-362.

[25]. Villa, I.M., De Bièvre, P., Holden, N.E. and Renne, P.R. (2015). IUPAC-IUGS recommendation on the half life of ^{87}Rb. Geochimica et Cosmochimica Acta. 164: 382-385.

[26]. Kemp, A.I.S., Hawkesworth, C.J., Foster, G.L., Paterson, B.A., Woodhead, J.D., Hergt, J.M., Gray, C.M and Whitehouse, M.J. (2007). Magmatic and crustal differentiation history of granitic rocks from hafnium and oxygen isotopes in zircon. Science. 315: 980-983.

[27]. Yang, J.H., Wu, F.Y., Wilde, S.A., Xie, L.W., Yang, Y.H. and Liu, X.M. (2007). Tracing magma mixing in granite genesis, in situ U–Pb dating and Hf-isotope analysis of zircons. Contrib. Miner. Petrol. 153: 177-190.

[28]. Hofmann, A.W. (1997). Mantle geochemistry: the message fromoceanic volcanism. Nature1. 385: 219-229.

[29]. Smith, E.I., Sánchez, A., Walker, J.D. and Wang, K. (1999). Geochemistry of mafic magmas in the Hurricane volcanic field, Utah: implications for small- and large-scale chemical variability of the lithospheric mantle. Journal of Geology. 107: 433-448.

[30]. Martin, H. (1987). Petrogenesis of Archaean trondhjemites, tonalites and granodiorites from eastern Finland: major and trace element geochemistry. Journal of Petrolog. 28: 921-953.

[31]. Nabatian, G., Ghaderi, M., Neubauer, F., Honarmand, M., Liu, X., Dong, Y., Jiang, S.Y., Quadt, A. and Bernroider, M. (2014). Petrogenesis of Tarom high-potassic granitoids in the Alborz-Azarbaijan belt, Iran: Geochemical, U-Pb zircon and Sr-Nd-Pb isotopic constraints. Lithos. 184: 324-345

[32]. Thirlwall, M.F., U.B.G. J. and Jenkins, C. (1994). Interaction between continental lithosphere and the Iceland Plume Sr-Nd-Pb isotope geochemistry of Tertiary basalts, NE Greenland. Journal of Petrology. 35: 839-879.

[33]. Baker, J.A., Menzies, M.A., Thirlwall, M.F. and MacPherson, C.G. (1997). Petrogenesis of Quaternary Intraplate Volcanism, Sana'a, Yemen: Implications for Plume-Lithosphere Interaction and Polybaric Melt Hybridization. Journal of Petrology. 38 (10): 1359-1390.

[34]. Muller, D., Rock, N.M.S. and Groves, D.I. (1992). Geochemical discrimination between shoshonitic and potassic volcanic rocks from different

tectonic setting: a pilot study. Mineralogy and Petrology. 46: 259-286.

[35]. Fang, N. and Niu, Y. (2003). Late Paleozoic ultramafic lavas in Yunnan, SW China, and their geodynamic significance. Journal of Petrolog. 44: 141-158.

[36]. Rossetti, F., Nasrabady, M., Vignaroli, G., Theye, T., Gerdes, A., Razavi, M.H. and Vaziri, H.M. (2010). Early Cretaceous migmatitic mafic granulites from the Sabzevar range (NE Iran): implications for the closure of the Mesozoic peri-Tethyan oceans in central Iran. Terra Nova. 22: 26-34.

[37]. Pearce, J.A. (1983). Role of the sub-continental lithosphere in magma genesis at active continental margins. In: Hawkesworth, C.J. and Norry, M.J. eds. Continental Basalts and Mantle Xenoliths. Nantwich, Cheshire: Shiva Publications. UK. pp. 230-250.

[38]. Cameron, B.I., Walker, J.A., Carr, M.J., Patino, L.C., Matias, O. and Feigenson, M.D. (2003). Flux versus decompression melting at stratovolcanos in southeastern Guatemala. Journal of Volcanology and Geothermal Research. 19: 21-50.

[39]. López-Moro, F.J. and López-Plaza, M. (2004). Monzonitic series from the Variscan Tormes Dome (Central Iberian Zone): petrogenetic evolution from monzogabbro to granite magmas. Lithos. 72: 19-44.

[40]. Li, X.H., Li, Z.X., Li, W.X., Liu, Y., Yuan, C., Wei, G.J. and Qi, C.S. (2007). U-Pb zircon, geochemical and Sr-Nd-Hf isotopic constraints on age and origin of Jurassic Iand A-type granites from central Guangdong, SE China: a major igneous event in response to foundering of a subducted flat-slab. Lithos. 96: 186-204.

[41]. Aydin, F., Karsli, O. and Chen, B. (2008). Petrogenesis of the Neogene alkaline volcanic with implications for post collisional lithospheric thinning of the Eastern Pontides, NE Turkey. Lithos. 104: 249-266.

ژئوشیمی، پترولوژی و کانی‌زایی سنگ‌های ولکانیکی جنوب نیشابور، شمال شرق ایران

اعظم انتظاری هرسینی‪¹‬، سید احمد مظاهری‪*¹‬، سعید سعادت‪²‬ و ژوزه فرانسیسکو سنتوز‪³‬

۱- گروه زمین‌شناسی، دانشگاه فردوسی مشهد، ایران

۲- گروه زمین‌شناسی، دانشگاه آزاد اسلامی واحد مشهد، ایران

۳- گروه زمین‌شناسی، دانشگاه آویرو، پرتغال

* نویسنده مسئول مکاتبات: mazaheri@ferdowsi.um.ac.ir

چکیده:

این تحقیق داده‌های جدیدی را در خصوص ژئوشیمی، ایزوتوپ‌های استرانسیوم و نئودیوم و همچنین کانه‌زایی سنگ‌های آتش‌فشانی جنوب نیشابور در شمال شرق ایران ارائه می‌دهد. بر اساس طبقه‌بندی شیمیایی سنگ‌های آتش‌فشانی منطقه مورد مطالعه در محدوده‌های تراکی آندزیت بازالت، تراکی آندزیت، تراکیت و تراکی داسیت قرار می‌گیرند. تجزیه ژئوشیمیایی این سنگ‌های آتش‌فشانی و نرمالیزه کردن آن‌ها نسبت به کندریت‌ها نشان‌دهنده غنی‌شدگی عناصر کمیاب سبک نسبت به عناصر کمیاب سنگین است و همچنین بی‌هنجاری منفی از عناصر نئوبیوم و تیتانیوم و بی‌هنجاری مثبت نسبت به اورانیوم را می‌توان در نمودارهای عنکبوتی نرمال شده به گوشته اولیه مشاهده کرد که این ویژگی‌ها متعلق به مناطق فرورانش می‌باشند. نمودارهای زمین ساختی خاستگاه این سنگ‌ها را کمان پس از برخورد معرفی می‌کند. مقدار اولیه $^{87}Sr/^{86}Sr$ از ۰/۷۰۴۰۸ تا ۰/۷۰۵۹۹۳ و مقدارNdi^ϵ از ۳/۳۴+ تا ۵+ برای چهار نمونه از سنگ‌های مورد مطالعه که مورد تجزیه ایزوتوپی قرار گرفتند متغیر می‌باشند که این مقادیر بیانگر منشأ گوشته‌ای است. در نهایت می‌توان به این نتیجه رسید که سنگ‌های آتش‌فشانی منطقه مورد مطالعه در یک محیط پس از برخورد به دنبال فرورانش اقیانوس تتیس جوان تشکیل شده‌اند. آثار کانی‌سازی زیادی را در سنگ‌های آتش‌فشانی منطقه مورد مطالعه می‌توان مشاهده کرد. از کانی‌های قابل مشاهده در منطقه به کانی‌های ثانویه مالاکیت، آتاکامیت و کوولیت و کانی‌های اولیه سولفید مس، کالکوسیت به مقدار فراوان و به مقدار جزئی بورنیت می‌توان اشاره کرد. کانی‌سازی بیشتر به صورت رگه- رگچه، پر کننده فضای خالی و به مقدار کمتر به صورت پراکنده در متن سنگ قرار دارد آنچه مشخص است کانی‌سازی اپی ژنتیک بوده و حرکت محلول‌های تشکیل‌دهنده آن‌ها توسط ساختارهای خطی و گسل‌ها کنترل می‌شود و این خصوصیات نشان‌دهنده کانی‌سازی از نوع هیدروترمال است. به مقدار فراوان دگرسانی کربناته در سنگ‌های آتش‌فشانی مورد مطالعه قابل مشاهده است و آثار دگرسانی آرژلیک در منطقه مشاهده نمی‌شود که این مسئله نشان می‌دهد که منشأ کانی زایی اولیه محلول هیدروترمالی با pH قلیایی است.

کلمات کلیدی: کالکوسیت، سنگ‌های آتش‌فشانی بعد از برخورد، ایزوتوپ‌های نئودیوم و استرانسیوم، نیشابور، شمال شرق ایران.